

PHYSICS-BASED SIMULATION OF MEGATHRUST GROUND MOTIONS AT 54 DAMS IN NEW ZEALAND

Michael Dupuis¹
Jake Faulkner²
Robin Lee³
Brendon Bradley⁴

ABSTRACT

Estimating ground motion from large-magnitude subduction earthquakes is critical for assessing seismic risk for dams near subduction zones. This study presents physics-based hybrid broadband simulations for 50 M_w8.7 rupture scenarios on the Hikurangi Subduction Zone in Aotearoa New Zealand, using subduction-specific parameter models validated with subduction interface events. Ground motions were simulated at 54 dam sites to support response history analysis and infrastructure risk assessment. The simulations reveal strong and spatially variable shaking, with characteristically long durations and high Arias intensities. Ground-motion intensity was found to be sensitive to rupture characteristics, including hypocentre location, subevent locations, rupture velocity, and stress parameter. These results provide critical insights for seismic hazard analysis, seismic structural response assessment, and resilience planning for dam infrastructure exposed to potential megathrust earthquakes.

INTRODUCTION

The Hikurangi subduction interface is a shallow dip reverse thrust fault under the North Island of New Zealand (NZ) which has formed between the Australian and Pacific plates (Barker et al., 2009). Although paleoearthquake evidence and recorded historic earthquakes collectively provide evidence for the potential of a very large megathrust earthquake on the Hikurangi Subduction Zone, possible rupture scenarios are relatively poorly constrained. No great earthquakes on the Hikurangi subduction interface have been observed in the historical period.

Empirical ground-motion models (GMMs) for subduction interface events (e.g., Parker, 2020) are widely used to provide ground-motion estimates for moderate- and large-magnitude earthquakes. However, such GMMs are based on limited global data—especially at larger magnitudes, and don't include explicit treatment of rupture characteristics which control ground motions from exceptionally large earthquakes, such as megathrust ruptures. Furthermore, empirical GMM are unable to produce acceleration time series which were needed for response history analysis of dams and other engineered structures. This contrasts with physics-based ground-motion simulation,

¹ Geosyntec Consultants Inc., Davis, California, michael.dupuis@geosyntec.com.

² University of Canterbury, Christchurch, New Zealand, jake.faulkner@canterbury.ac.nz.

³ University of Canterbury, Christchurch, New Zealand, robin.lee@canterbury.ac.nz.

⁴ University of Canterbury, Christchurch, New Zealand, brendon.bradley@canterbury.ac.nz.

which can directly apply advancements validated on smaller magnitudes, while also providing explicit treatment of phenomenologically important rupture characteristics. Physics-based simulations can produce triaxial acceleration time series needed for engineering analysis and thus provides additional value beyond pure estimation of RotD50 ground motion intensity metrics (IMs).

In this paper, physics-based ground-motion simulation is used to produce realistic ground motions for dams across NZ for megathrust rupture scenarios on the Hikurangi Subduction Zone. We use subduction-specific simulation models that have been validated with small- (Dupuis et al., 2025) and moderate-magnitude interface ground motions in the same geographic region. First, the details of the simulation method, its input models and parameters, and computational details are then discussed. Next, NZ-wide ground-motions and their sensitivities to rupture properties are presented. Finally, ground motions for 54 dams across NZ are presented and discussed.

SIMULATION METHOD AND INPUTS

In this section, the ground-motion simulation method and computational details of the simulations are presented followed by the treatment of rupture geometry, subevents, variability, and the resulting rupture kinematics.

Hybrid broadband method

The Graves and Pitarka (Graves and Pitarka, 2010; Pitarka et al., 2022) hybrid broadband ground-motion simulation method was applied. This approach combines a comprehensive finite-difference solution to 3D wave propagation at low frequencies with a simplified-physics approach at high frequencies. The low- and high-frequency (LF and HF, respectively) components are combined using a set of matched 4th order Butterworth filters to produce broadband ground-motion waveforms with usable content from 0–50 Hz from which spectral ordinates from 0–10 s can readily be computed. RotD50 ground-motion intensity metrics (IMs) were considered to facilitate comparison with empirical GMMs for subduction interface earthquakes.

Computational details

The simulations utilized a 3D finite difference grid 950 km long, 500 km wide, and 70 km deep oriented to encapsulate the rupture extent and cities on the North and South Islands of NZ, as shown in Figure 1. A grid spacing of 0.1 km was used with a minimum shear wave velocity, $V_{S,\min} = 500$ m/s, which was able to resolve frequencies up to 1.0 Hz in the low-frequency component and resulted in 33.25 billion spatial grid points in the velocity model domain. Material properties from the New Zealand Velocity Model (NZVM) v2.08 by Thomson et al. (2020) were used with a squashed topographic representation and incorporation of sedimentary basins. The simulation duration was set to be $T_{\max} = 240$ s with a time step of $dt = 0.005$ s resulting in 48,000 time steps for each simulation. Ground motion time series were extracted across uniform surface grid with 4 km spacing which was supplemented by denser non-uniform grids in population centres.

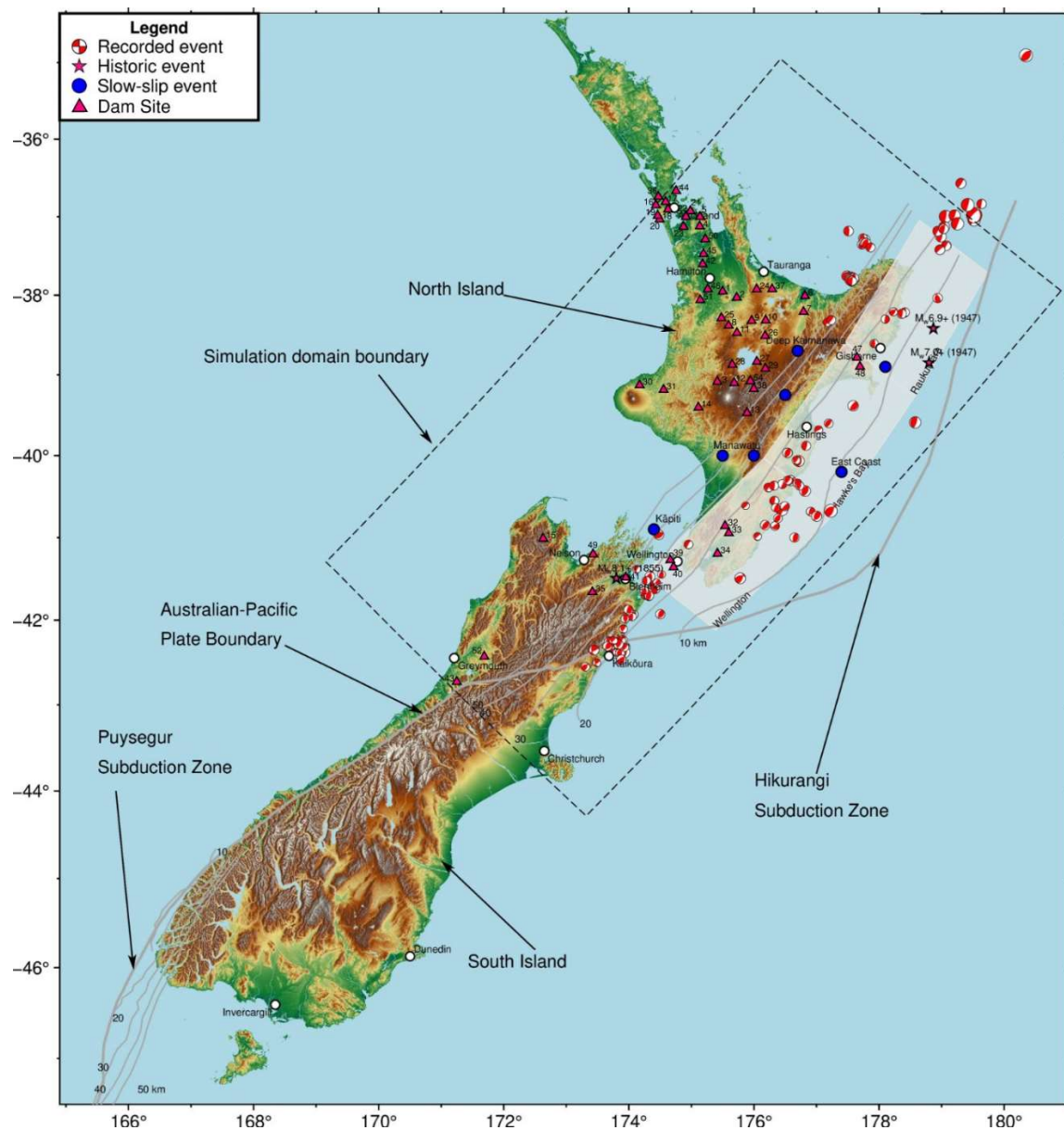


Figure 1. Locations of 54 dams considered shown with selected recorded events, large historic events (Doser and Webb, 2003), slow-slip events (Wallace, 2020), and regional population centres.

Rupture geometry

The 2022 NZ National Seismic Hazard Model (NSHM) allows for non-characteristic, variable rupture geometries; however, we limited our analysis to a single background rupture extent to reduce computational demand. For all $M_w 8.7$ Hikurangi megathrust rupture scenarios we adopted the 2010 NZ NSHM geometry, with maximum rupture extents, which was used by Bayless et al. (2019) and thus forms a convenient baseline. This includes three rupture segments: (i) Raukumara (north), (ii) Hawke's Bay (central), and (iii) Wellington (south) as shown in Figure 1.

The southern limit of the rupture is at the transition zone between the Marlborough fault system and the Hikurangi Subduction Zone due to fault system interactions at this transitional plate boundary (Pizer, 2021). The northern limit of the rupture is defined offshore. Although ruptures extending further northward toward Tonga are possible, further northeastward propagation is unlikely to significantly affect ground motions in NZ. Therefore, the northern limit is a pragmatic, albeit arbitrary, selection. The background rupture is 124 km wide and 618 km long.

Subevents

Four 40 km wide, 70 km long, M_w 7.7 subevents were placed on the deeper portions of background rupture. For the archetype scenario rupture, the subevents were placed with their geometric centres at 75% of the background rupture width down-dip from the top of the background rupture and with 183 km centre-to-centre spacing along-strike, with the subevent array centered on the background rupture and sides aligned with the background rupture edges.

Several properties of the subevents were scaled relative to the background rupture based on observed subevent characteristics collated from studies of global megathrust ruptures. Subevent slip was doubled relative to the background rupture and rise time was halved. These two effects result in four times greater average slip velocity on the subevents compared with on the background rupture, a convenient result which was similar to forensic studies of Maule (Frankel, 2017). Finally, the subevent stress parameter was increased by a factor of six, compared with the background rupture stress parameter. Other parameters, such as rupture velocity, coefficient of variation of slip, and slip correlation lengths were specified to be the same on the subevents as on the background rupture.

DAM SITE CHARACTERISTICS

Dam locations and properties were provided by Lehner et al. (2024) in the Global Dam Watch (GDW) database. The GDW database provides a harmonized, geospatially explicit global repository of 41,145 river barriers and 35,295 associated reservoirs, integrating and curating multiple existing global and regional datasets into a consistent format. Each record includes over 50 dam and reservoir attributes, such as dam height, year of construction, primary purpose, storage volume, discharge, and installed hydropower capacity, when available. Selected dam metadata for 54 NZ dams located within the simulation velocity model domain is provided in Table 1. Site and path parameters, which express the shear wave velocity at each dam and various measures of distances to the rupture, were computed from the dam location, NZVM, and the rupture model, and are provided in Table 2.

Table 1. Selected metadata information for the 54 dams considered (Lehner et al, 2024).

ID	GDW ID	Name	River	Year Built	Height (m)	Length (m)	Longitude (degrees)	Latitude (degrees)
1	2105	Karapiro	Waikato	1947	67	332	175.54	-37.92
2	2106	Arapuni	Waikato	1928	64	94	175.66	-38.05
3	2107	Poutu	Poutu	1972	13	150	175.75	-39.06
4	5500	Upper Mangatawhiri	Mangatawhiri	1965	35	494	175.16	-37.08
5	5503	Mangatangi	Mangatangi	1977	78	340	175.21	-37.11
6	5521	Matahina	Rangataiki	1965	86	345	176.82	-38.12
7	5525	Aniwhenua Barrage	Rangitaiki	1980	13	400	176.79	-38.31
8	5526	Maraetai	Waikato	1953	87	133	175.75	-38.35
9	5527	Atiamuri	Waikato	1958	44	437	176.02	-38.39
10	5528	Ohakuri	Waikato	1960	49	150	176.09	-38.41
11	5529	Whakamaru	Waikato	1956	56	337	175.81	-38.42
12	5530	Otamangakau	Otamanakau Stream	1971	20	260	175.62	-39.01
13	5531	Moawhango	Moawhango	1975	68	325	175.75	-39.41
14	5532	Patea	Patea	1984	82	190	174.56	-39.54
15	5534	Cobb	Cobb	1954	33	221	172.68	-41.11
16	6820	Waitakere	Waitekere	1928	25	175	174.53	-36.90
17	6822	Upper Nihotupu	Nihotupu	1923	50	162	174.56	-36.95
18	6823	Lower Nihotupu	Nihotupu	1948	25	381	174.61	-36.96
19	6824	Upper Huia	Huia Stream	1928	37	166	174.54	-36.96
20	6825	Lower Huia	Huia Stream	1971		366	174.57	-36.99
21	6826	Cossey's	Cossey's Creek	1955	41	168	175.11	-37.06
22	6827	Hays Creek	Hays	1964	26	60	175.02	-37.07
23	6828	Wairoa	Wairoa	1975	47	213	175.12	-37.10
24	6832	McLaren Falls	Mangapapa	1925	38	—	176.04	-37.81
25	6833	Waipapa	Waikato	1961	37	283	175.68	-38.29
26	6835	Taupo Lake Control	Waikato		—	—	176.13	-38.62
27	6836	Hinemaiaia B	Hinemaiaia	1966	22	75	176.06	-38.87
28	6837	Kuratau	Kuratau	1962	16	43	175.73	-38.87
29	6838	Hinemaiaia A	Hinemaiaia	1952	12	90	176.09	-38.89
30	6839	Mangamahoe	Mangamahoe	1931	24	154	174.13	-39.12
31	6840	Ratapiko	Mako	1926	17	85	174.33	-39.21
32	6841	Te Marua 1	Hutt	1986	15	1500	175.15	-41.08
33	6842	Te Marua 2	Hutt	1985	15	1600	175.15	-41.09
34	6843	Morton	Wainuiomata	1911	17	164	175.00	-41.26
35	6845	Waihopai	Waihopai	1927	37	272	173.57	-41.66
36	7305	Nihotupu Auxiliary Dam	Nihotupu	1921	20	84	174.56	-36.93
37	7306	Raymond	Paraita	1962	18	50	176.24	-37.85
38	7307	Rangipo	Tongariro	1980	20	108	175.78	-39.21
39	7308	Lower Karori	Kaiwharawhara	1872	26	128	174.75	-41.29
40	7309	Upper Karori	Kaiwharawhara	1908	27	98	174.74	-41.30
41	7310	Taylor	Taylor	1965	22	—	173.93	-41.57
42	10808	—	—	—	—	—	175.12	-37.48
43	10816	—	—	—	—	—	171.20	-42.66
44	24852	—	—	—	—	—	174.71	-36.74
45	24865	—	—	—	—	—	175.18	-37.49
46	24881	—	—	—	—	—	175.29	-37.95
47	24885	—	—	—	—	—	177.78	-38.86
48	24886	—	—	—	—	—	177.77	-38.87
49	24896	—	—	—	—	—	173.37	-41.29
50	25225	—	—	1991	—	—	175.16	-37.27
51	25229	—	—	—	—	—	175.22	-37.94
52	25414	—	—	—	—	—	171.41	-42.53
53	29884	—	—	—	—	—	175.78	-38.97
54	41133	—	—	—	—	—	175.82	-39.13

Table 2. Site and path parameters for the 54 dams considered. For a description of terms refer to Kaklamanos et al (2011). X_{ba} is the site backarc distance from the fault at the surface measured perpendicular to the strike of the fault.

ID	V _{s30} (m/s)	R _{jb} (km)	R _{rup} (km)	R _x (km)	R _y (km)	R _{hypo} (km)	R _{epi} (km)	X _{ba} (km)
1	500	181	182	304	58	238	237	200
2	500	166	165	287	54	220	219	183
3	500	113	94	214	-27	136	134	111
4	455	261	263	385	107	335	334	282
5	455	255	257	379	108	329	329	276
6	691	76	79	198	111	176	175	97
7	500	64	70	188	93	155	154	86
8	691	149	139	260	33	188	188	157
9	691	125	117	238	45	171	170	135
10	691	118	111	232	46	166	165	129
11	500	143	131	252	30	179	179	148
12	500	122	106	227	-29	148	147	123
13	691	77	72	191	-56	120	119	88
14	455	144	136	256	-130	218	218	163
15	455	132	136	253	-357	407	406	184
16	691	317	322	444	87	382	382	339
17	635	311	317	439	85	376	375	334
18	455	307	312	434	87	372	372	329
19	635	312	318	440	83	376	375	334
20	635	309	314	436	83	372	372	331
21	455	266	269	390	106	339	339	287
22	455	271	275	397	100	342	342	293
23	383	262	265	387	103	335	334	284
24	691	149	153	274	95	228	227	171
25	691	156	148	269	34	197	196	166
26	691	113	95	216	31	145	144	112
27	691	123	85	205	5	128	127	102
28	691	133	107	228	-12	149	148	124
29	691	120	81	201	6	124	123	98
30	221	199	196	317	-118	263	263	221
31	455	179	177	297	-114	244	243	201
32	455	0	20	96	-232	228	228	21
33	455	0	20	96	-232	229	228	21
34	454	0	19	91	-255	251	251	19
35	455	57	63	159	-360	371	371	87
36	635	313	318	440	87	378	378	335
37	691	133	136	257	102	217	216	155
38	691	96	82	202	-38	126	124	99
39	557	0	21	103	-269	268	268	34
40	516	0	21	103	-271	269	269	34
41	316	26	37	136	-335	341	341	70
42	500	238	242	364	72	300	299	259
43	279	282	281	348	-560	596	595	172
44	455	315	318	440	111	387	387	336
45	500	232	237	359	74	295	295	254
46	500	200	198	320	42	248	248	216
47	455	0	18	82	97	109	108	-20
48	455	0	18	83	97	109	107	-20
49	456	71	76	192	-339	363	363	125
50	413	247	252	373	92	317	316	270
51	500	206	204	326	40	253	253	222
52	487	260	259	329	-539	573	573	168
53	500	122	98	218	-18	139	138	115
54	691	104	84	204	-29	126	125	101

SIMULATION RESULTS

In this section, the simulated ground motions for the various M_w 8.7 rupture scenarios are examined. First, the simulated ground motions from the archetype scenario are used to illustrate the effect of subevent locations on predicted ground motions. Next, the results from all simulations are presented to show average intensities and trends across NZ. Finally, ground motions at 54 dams in NZ are summarized and presented.

Archetype scenario ground motions

Figure 2 provides the archetype scenario ground motion records. Figure 3 illustrates selected IMs for the archetype scenario, including PGA, 5–75% significant duration, $D_s(5-75\%)$, Arias intensity (AI), and pseudo-spectral accelerations at period T, pSA(T). Viewing the results through this lens is helpful to demonstrate the effect of the rupture features, e.g., subevent locations, on simulated ground motions.

At short periods, e.g., $T = 0.2$ s, the most intense shaking occurs in proximity to the subevents along the east coast of the North Island. This geospatial pattern, with stronger motions near and weaker motions between subevents, underscores the importance of subevent locations. These trends persist to longer periods, e.g., 1.0 s however, at very long periods, e.g., 3.0 s, proximity to subevents appears to have a small effect (i.e., approximately 10%). The archetype simulation motions exhibit very large changes in AI over relatively short distances. AI directly above subevents is very large (e.g., greater than 30 m/s) while AI between subevents is relatively small (e.g., 5 m/s or less).

Mean simulated ground motions

Figure 4 illustrates the geometric mean of the simulated ground motions for selected IMs. The results show very large pseudo-spectral accelerations at $T = 0.2$ s, pSA(0.2 s), greater than 1.2 g along the entire eastern coastline of the North Island. The results also exhibit large geospatial variations of Arias intensity, with large arias intensities of 10 m/s or larger for most of the surface projection of the background rupture, which corresponds to areas with strong-motion-generating subevents.

Dam ground motions

Figure 5 compares the simulated response spectra from the 50 scenarios with empirical GMM predictions for 6 of the tallest dams of the 54 dams within the velocity model domain. The results indicate a strong consistency between the mean simulation prediction and the empirical GMM predictions. The simulations demonstrate approximately an order-of-magnitude variation in IM amplitudes between scenarios.

Table 3 summarizes selected IMs for the 54 dams considered. The results indicate very intense and highly variable ground motions for seven dams: Te Marua 1 (ID 32) and 2 (ID 33), Morton (ID 34), Lower (ID 39) and Upper Karori (ID 40), and two unnamed dams (ID 47 and 48). Shaking is significantly less intense at all other dams.

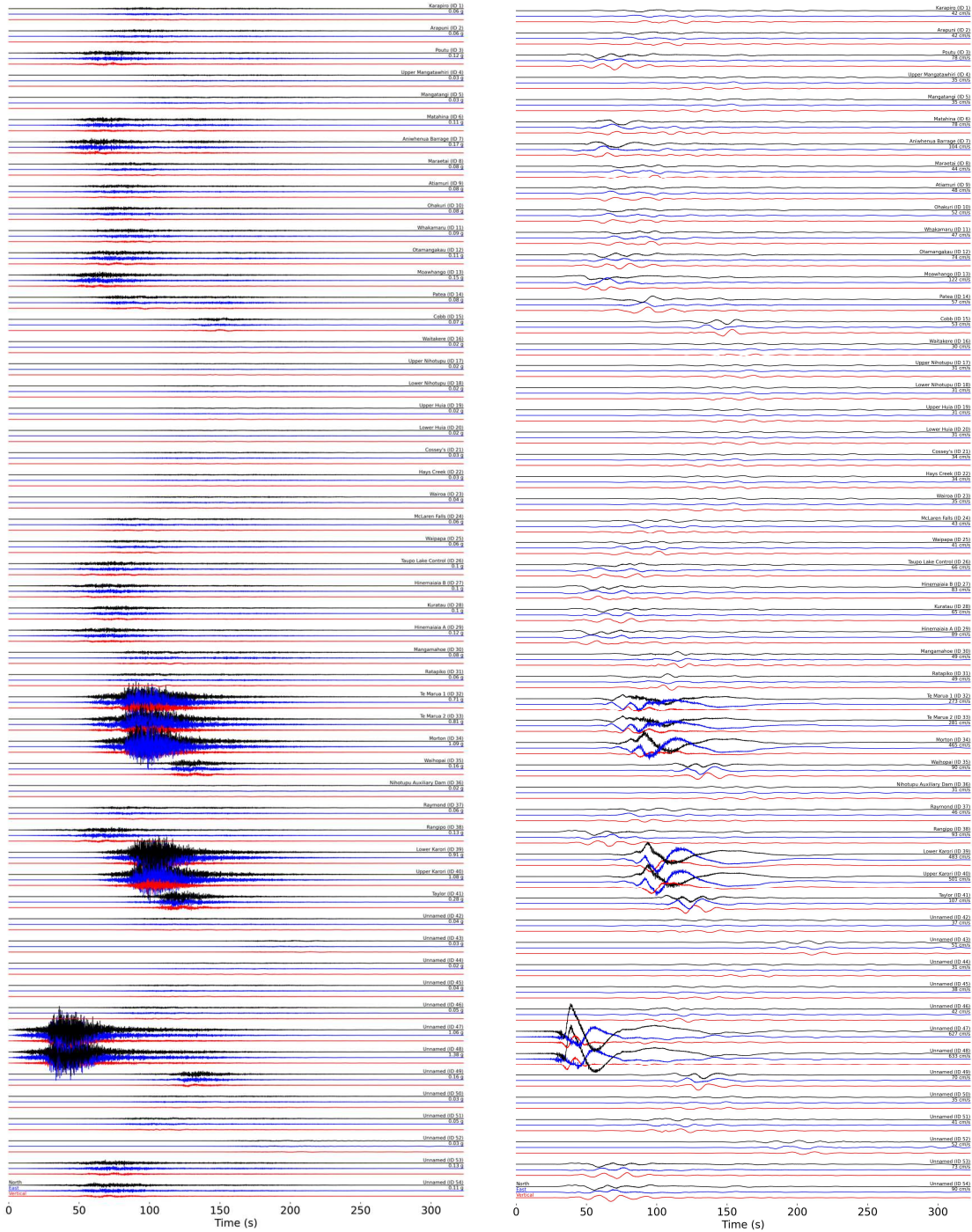


Figure 2. Archetype scenario simulation ground-motion records for all 54 dams within the simulation velocity model domain: (left) acceleration time series, (right) velocity time series. Peak ground acceleration and peak ground velocity (RotD50) are labelled for each dam. North, east, and vertical components are shown in black, blue, and red, respectively. Dams are shown by ID number in ascending order from top to bottom.

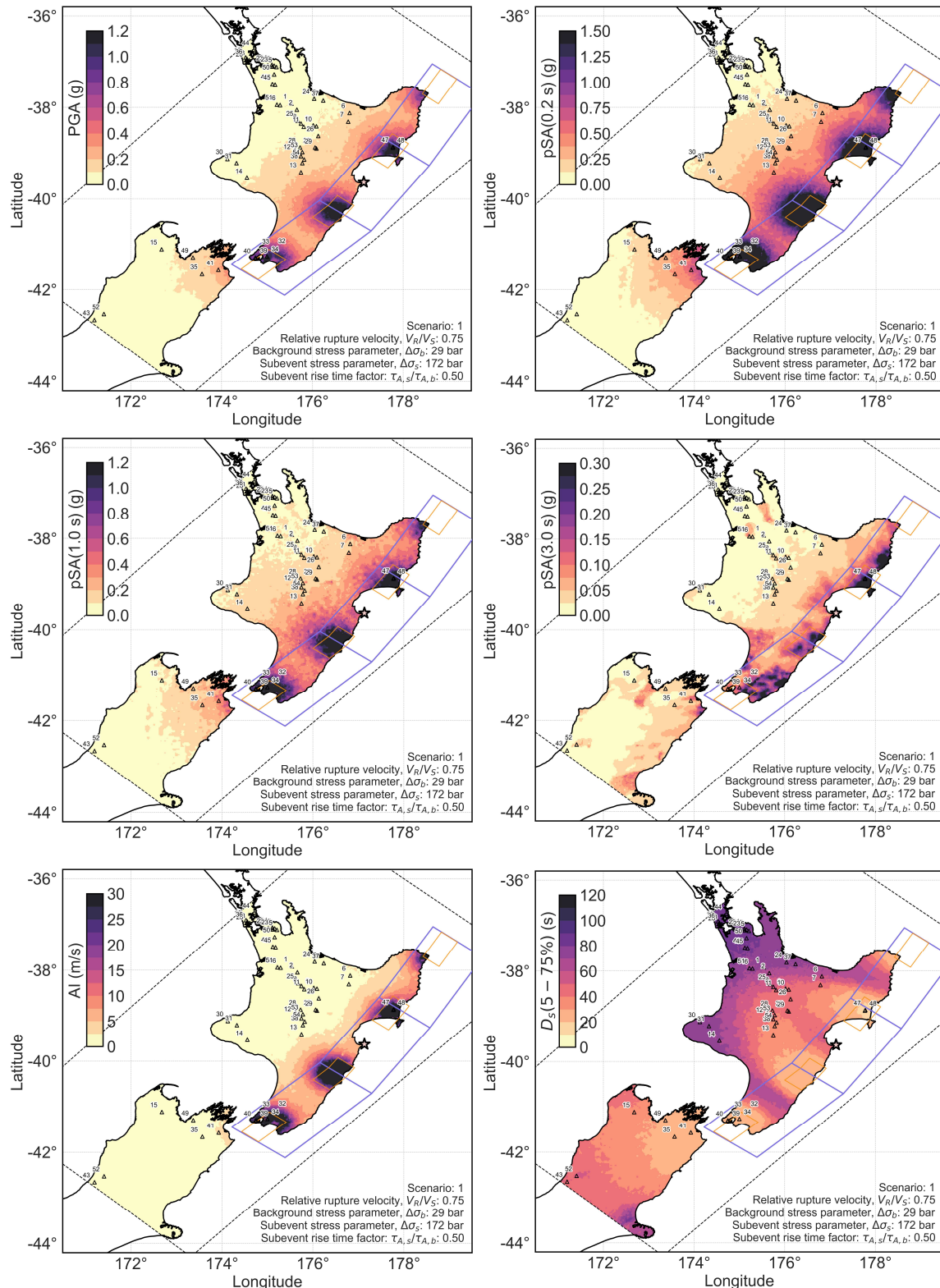


Figure 3. Archetype scenario simulation ground-motion predictions: (top left) PGA, (top right) pSA(0.2 s), (middle left) pSA(1.0 s), (middle right) pSA(3.0 s), (bottom left) AI, and (bottom right) $D_s(5 - 75\%)$.

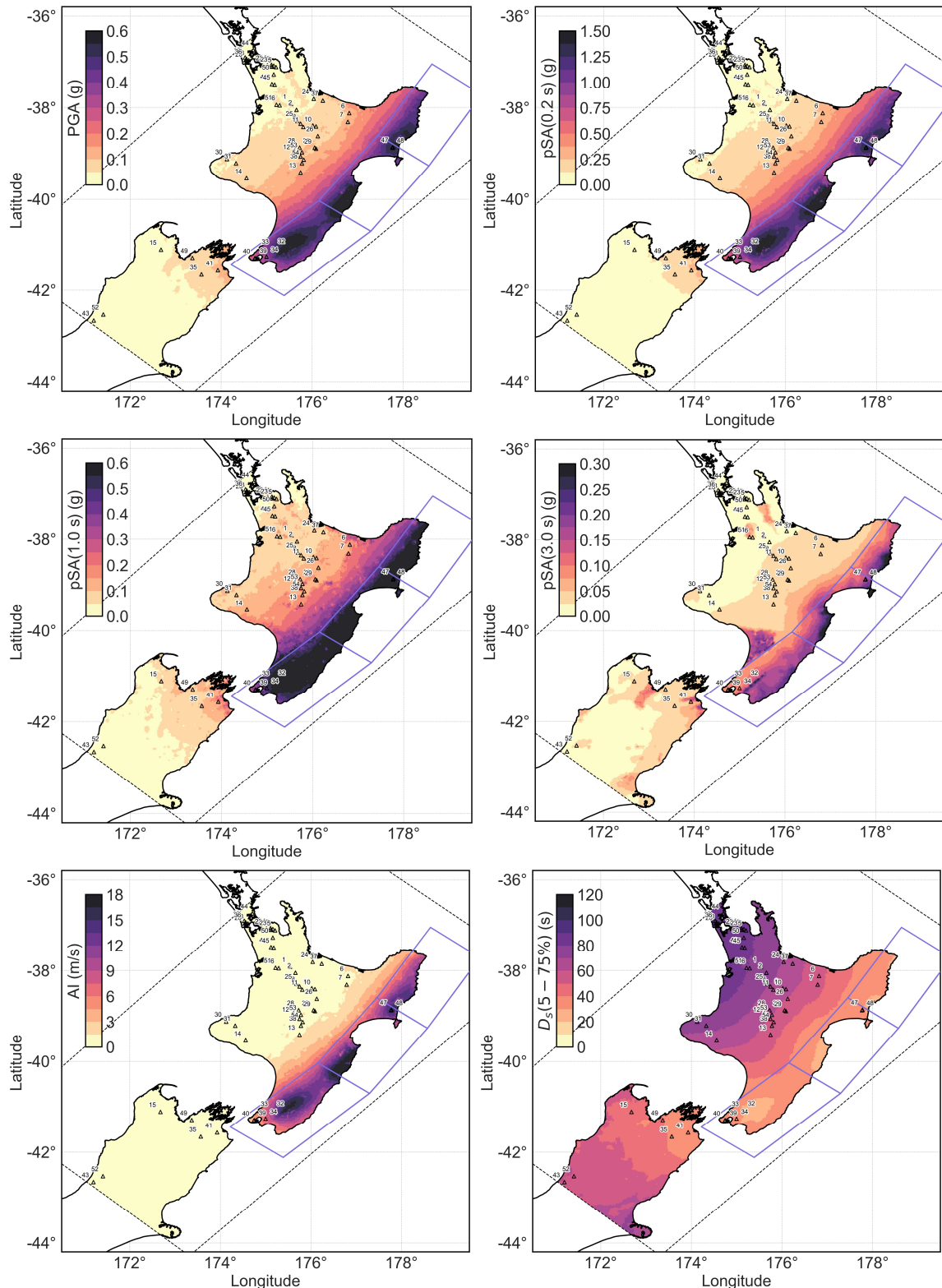


Figure 4. Geometric mean of simulation ground-motion predictions from all scenarios: (top left) PGA, (top right) pSA(0.2 s), (middle left) pSA(1.0 s), (middle right) pSA(3.0 s), (bottom left) AI, and (bottom right) D_s (5-75%).

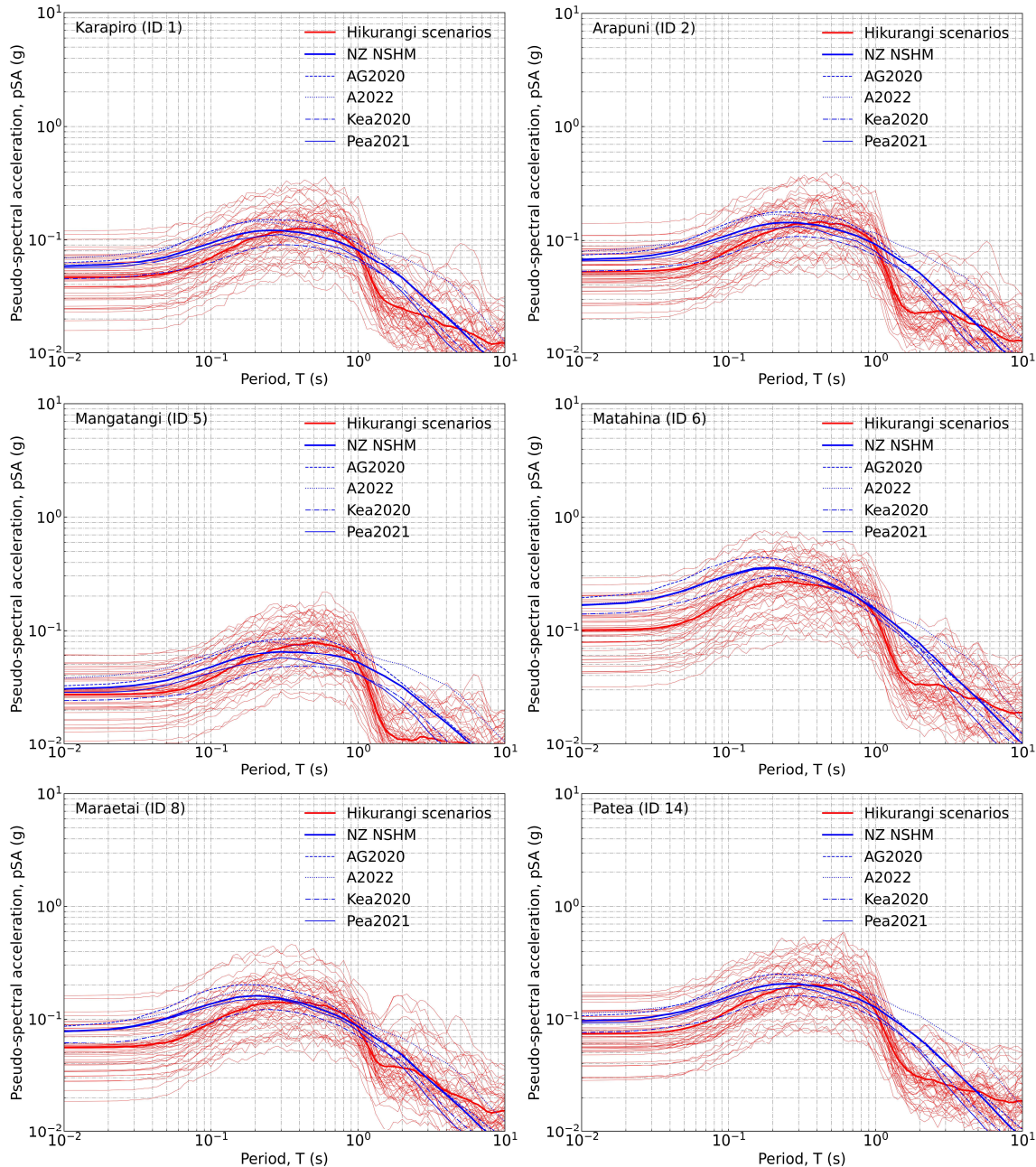


Figure 5. Simulation and empirical predictions: NZ NSHM (Bradley et al., 2024), AG2020 (Abrahamson and Gülerce, 2020), A2022 (Atkinson, 2024), Kea2020 (Kuehn et al., 2020), and Pea2021 (Parker et al., 2020), for Karapiro (top left), Arapuni (top right), Mangatangi (middle left), Matahina (middle right), Maraetai (bottom left), and Patea (bottom right) with the mean (simulation) predictions shown in bold.

Table 3. Ground motions for the 54 dams from the 50 scenarios simulated: peak ground acceleration, PGA; Arias intensity, AI; and 5–75% significant duration, Ds(5-75%).

ID	Name	PGA (g)			AI (m/s)			Ds(5-75%) (s)		
		Min.	Mean	Max.	Min.	Mean	Max.	Min.	Mean	Max.
1	Karapiro	0.02	0.05	0.12	0.03	0.23	1.11	49	76	138
2	Arapuni	0.02	0.05	0.14	0.04	0.29	1.44	47	74	132
3	Poutu	0.03	0.11	0.28	0.14	0.94	4.56	40	59	94
4	Upper Mangatawhiri	0.01	0.03	0.06	0.01	0.08	0.44	58	83	148
5	Mangatangi	0.01	0.03	0.06	0.01	0.09	0.46	58	82	151
6	Matahina	0.03	0.10	0.29	0.10	0.71	3.53	29	53	103
7	Aniwhenua Barrage	0.04	0.13	0.39	0.21	1.20	6.45	30	53	110
8	Maraetai	0.02	0.06	0.16	0.04	0.28	1.53	44	69	125
9	Atiamuri	0.02	0.07	0.17	0.05	0.38	1.73	40	64	120
10	Ohakuri	0.02	0.07	0.19	0.06	0.42	2.23	42	63	120
11	Whakamaru	0.03	0.07	0.19	0.08	0.50	2.41	45	68	124
12	Otamangakau	0.03	0.10	0.24	0.12	0.80	3.99	41	62	97
13	Moawhango	0.04	0.11	0.33	0.14	0.93	5.42	35	54	87
14	Patea	0.03	0.07	0.17	0.10	0.51	2.55	43	65	101
15	Cobb	0.01	0.04	0.11	0.02	0.10	0.64	30	47	118
16	Waitakere	0.01	0.01	0.03	0.00	0.03	0.12	66	90	146
17	Upper Nihotupu	0.01	0.02	0.04	0.00	0.03	0.16	63	90	148
18	Lower Nihotupu	0.01	0.02	0.04	0.01	0.05	0.22	62	89	146
19	Upper Huia	0.01	0.02	0.03	0.00	0.03	0.15	61	91	147
20	Lower Huia	0.01	0.02	0.03	0.00	0.03	0.15	63	90	147
21	Cossey's	0.01	0.03	0.06	0.01	0.08	0.41	59	84	146
22	Hays Creek	0.01	0.02	0.06	0.01	0.07	0.38	58	84	149
23	Wairoa	0.01	0.03	0.07	0.01	0.10	0.53	59	83	144
24	McLaren Falls	0.02	0.05	0.12	0.03	0.21	1.03	43	69	132
25	Waipapa	0.02	0.05	0.14	0.03	0.25	1.36	46	71	126
26	Taupo Lake Control	0.03	0.08	0.22	0.07	0.54	3.08	36	60	110
27	Hinemaiaia B	0.03	0.09	0.28	0.09	0.68	4.04	34	56	100
28	Kuratau	0.03	0.08	0.20	0.08	0.51	2.57	41	62	96
29	Hinemaiaia A	0.03	0.10	0.29	0.10	0.74	4.36	33	55	89
30	Mangamahoe	0.03	0.07	0.16	0.11	0.51	2.15	48	76	112
31	Ratapiko	0.02	0.05	0.12	0.06	0.29	1.35	43	73	111
32	Te Marua 1	0.09	0.46	2.27	0.71	10.48	179.09	18	30	86
33	Te Marua 2	0.09	0.47	2.44	0.72	10.55	185.91	17	30	84
34	Morton	0.08	0.38	2.68	0.51	7.15	161.31	13	32	84
35	Waihopai	0.02	0.07	0.25	0.05	0.29	2.31	19	39	117
36	Nihotupu Auxiliary Dam	0.01	0.01	0.03	0.00	0.03	0.14	67	91	148
37	Raymond	0.02	0.06	0.16	0.04	0.27	1.40	41	65	124
38	Rangipo	0.03	0.10	0.29	0.11	0.77	4.05	37	56	90
39	Lower Karori	0.05	0.28	1.68	0.36	3.92	71.85	13	33	91
40	Upper Karori	0.06	0.29	1.68	0.40	4.07	63.88	13	33	95
41	Taylor	0.03	0.12	0.38	0.13	0.78	4.96	18	36	108
42	—	0.01	0.03	0.07	0.01	0.10	0.48	56	83	146
43	—	0.01	0.02	0.04	0.01	0.03	0.15	40	59	118
44	—	0.01	0.02	0.04	0.01	0.04	0.23	63	88	153
45	—	0.01	0.03	0.07	0.02	0.11	0.56	54	83	146
46	—	0.02	0.05	0.13	0.05	0.27	1.22	47	74	132
47	—	0.13	0.55	2.29	1.54	15.56	146.79	18	31	80
48	—	0.13	0.56	2.20	1.45	15.22	164.96	15	31	81
49	—	0.02	0.06	0.23	0.04	0.24	1.96	20	41	109
50	—	0.01	0.03	0.08	0.02	0.12	0.61	58	83	146
51	—	0.02	0.05	0.11	0.04	0.25	1.08	55	77	127
52	—	0.01	0.02	0.05	0.01	0.04	0.16	35	55	109
53	—	0.04	0.10	0.25	0.13	0.88	4.38	40	60	96
54	—	0.03	0.10	0.26	0.11	0.72	3.74	37	57	91

DISCUSSION AND CONCLUSIONS

In this study, physics-based ground-motion simulations were applied to the problem of ground-motion prediction at 54 dams in New Zealand for a Hikurangi megathrust earthquake. The simulations used subduction-specific source properties previously validated for small- (Dupuis et al., 2025) and moderate-magnitude earthquakes. In total, simulation of 50 different rupture scenarios was completed to investigate the sensitivity of the predicted ground motions to salient rupture properties.

The results indicate very large sensitivity of ground motions to the specific manifestation of each rupture scenario (e.g., subevent locations and rupture characteristics). In general, an order-of-magnitude difference in ground motion amplitudes were observed between rupture scenarios at a given dam. This finding, and the associated uncertainty in seismic hazard which it implies poses a challenge for engineers and planners charged with mitigating dam safety risk.

Seven dams were identified as having significantly more intense ground motions than the other 47 dams considered in this study. These dams which are anticipated to experience very intense ground motions are Te Marua 1 (ID 32) and 2 (ID 33), Morton (ID 34), Lower (ID 39) and Upper Karori (ID 40), and two unnamed dams (ID 47 and 48). Shaking is significantly less intense at all other dams.

All simulated ground motion records, supporting data files, and summary figures are available for download from <https://doi.org/10.17605/OSF.IO/WV738>.

ACKNOWLEDGEMENTS

The authors would like to gratefully acknowledge the New Zealand eScience Infrastructure (NeSI) [nesi00213], the Texas Advanced Computing Center (TACC), and the Korea Institute of Science and Technology Information (KISTI) [KSC-2023-CRE-0459] for the high-performance computing resources provided.

This work was financially supported by the University of Canterbury, QuakeCoRE: The NZ Centre for Earthquake Resilience, Resilience to Nature's Challenges National Science Challenge, the Marsden Fund, the New Zealand Natural Hazards Commission, and the Commonwealth Scholarship and Fellowship Plan funded by the Government of Canada.

REFERENCES

- Abrahamson, N., and Z. Gülerce. 2020. “Regionalized ground-motion models for subduction earthquakes based on the NGA-SUB database.” PEER Report 25.
- Atkinson, G.M. 2024. “Backbone ground-motion models for crustal, interface, and slab earthquakes in New Zealand from equivalent point-source concepts.” *Bulletin of the Seismological Society of America* 114 (1): 350–372.
- Barker, D.H.N., R. Sutherland, S. Henrys, and S. Bannister. 2009. “Geometry of the Hikurangi subduction thrust and upper plate, North Island, New Zealand.” *Geochemistry, Geophysics, Geosystems* 10 (2).
- Bradley, B.A., S.S. Bora, R.L. Lee, E.F. Manea, M.C. Gerstenberger, P.J. Stafford, G.M. Atkinson, G. Weatherill, J. Hutchinson, C.A. de la Torre, et al. 2024. “The ground-motion characterization model for the 2022 New Zealand National Seismic Hazard Model.” *Bulletin of the Seismological Society of America* 114 (1): 329–349.
- Clark, K., J. Howarth, N. Litchfield, U. Cochran, J. Turnbull, L. Dowling, A. Howell, K. Berryman, and F. Wolfe. 2019. “Geological evidence for past large earthquakes and tsunamis along the Hikurangi subduction margin, New Zealand.” *Marine Geology* 412: 139–172.
- Doser, D.I., and T.H. Webb. 2003. “Source parameters of large historical (1917–1961) earthquakes, North Island, New Zealand.” *Geophysical Journal International* 152 (3): 795–832.
- Dupuis, M., R. Lee, and B. Bradley. 2025. “Hybrid broadband ground-motion simulation validation of small-magnitude subduction earthquakes in New Zealand.” *Earthquake Spectra* (accepted). doi:10.1177/87552930251353816.
- Frankel, A. 2013. “Rupture history of the 2011 M9 Tohoku Japan earthquake determined from strong-motion and high-rate GPS recordings: Subevents radiating energy in different frequency bands.” *Bulletin of the Seismological Society of America* 103 (2B): 1290–1306.
- Frankel, A. 2017. “Modeling strong-motion recordings of the 2010 Mw8.8 Maule, Chile, earthquake with high stress-drop subevents and background slip.” *Bulletin of the Seismological Society of America* 107 (1): 372–386.

Graves, R.W., and A. Pitarka. 2010. “Broadband ground-motion simulation using a hybrid approach.” *Bulletin of the Seismological Society of America* 100 (5A): 2095–2123.

Kaklamanos, J., L.G. Baise, and D.M. Boore. 2011. “Estimating unknown input parameters when implementing the NGA ground-motion prediction equations in engineering practice.” *Earthquake Spectra* 27 (4): 1219–1235.

Kuehn, N., Y. Bozorgnia, K.W. Campbell, and N. Gregor. 2020. “Partially non-ergodic ground-motion model for subduction regions using the NGA Subduction database.” PEER Report 6.

Lehner, B., P. Beames, M. Mulligan, et al. 2024. “The Global Dam Watch database of river barrier and reservoir information for large-scale applications.” *Scientific Data* 11: 1069. <https://doi.org/10.1038/s41597-024-03752-9>.

Parker, G.A., J.P. Stewart, D.M. Boore, G.M. Atkinson, and B. Hassani. 2020. “NGA-Subduction global ground-motion models with regional adjustment factors.” PEER Report 3.

Pitarka, A., R. Graves, K. Irikura, K. Miyakoshi, C. Wu, H. Kawase, A. Rodgers, and D. McCallen. 2022. “Refinements to the Graves–Pitarka Kinematic Rupture Generator, Including a Dynamically Consistent Slip-Rate Function, Applied to the 2019 Mw 7.1 Ridgecrest Earthquake.” *Bulletin of the Seismological Society of America* 112 (1): 287–306.

Thomson, E.M., B.A. Bradley, and R.L. Lee. 2020. “Methodology and computational implementation of a New Zealand Velocity Model (NZVM2.0) for broadband ground-motion simulation.” *New Zealand Journal of Geology and Geophysics* 63 (1): 110–127.

Wallace, L.M. 2020. “Slow slip events in New Zealand.” *Annual Review of Earth and Planetary Sciences* 48: 175–203.